Detection of cracks in rotor based on the 2X and 3X super-harmonic frequency components and the crack-unbalance interactions

Jean-Jacques Sinou

Detection of cracks in rotor based on the $2\times$ and $3\times$ super-harmonic frequency components and the crack-unbalance interactions

Jean-Jacques Sinou
Laboratoire de Tribologie et Dynamique des Systèmes UMR-CNRS 5513
Ecole Centrale de Lyon, 36 avenue Guy de Collongue
69134 Ecully Cedex, France
email: jean-jacques.sinou@ec-lyon.fr

Abstract

The purpose of this paper is to investigate the use of the $2\times$ and $3\times$ super-harmonic components for detecting the presence of a single transverse breathing crack in a non-linear rotor system. This procedure is based on the detection of the super-harmonic components of the non-linear dynamical behaviour at the associated sub-critical resonant peaks.
The non-linear behaviour of the rotor system with a breathing crack is briefly analysed numerically: it will be illustrated that the effects of the crack size and location induce the variation of non-linear responses and the emerging of new resonance - antiresonance peaks of the cracked rotor at second, third and fourth harmonic component. Then, the influence of the crack-unbalance interactions and more particularly the relative orientation between the front crack and the unbalance are also undertaken with considerations of various crack depths, and unbalance magnitudes. It is demonstrated that for a given crack depth, the unbalance does not only affect the vibration amplitude of the $1\times$ amplitudes, but also the $\frac{1}{2}$ and $\frac{1}{3}$ sub-critical resonant peaks. Finally, it is illustrated that the emerging of super-harmonic components provides useful information on the presence of crack and may be used on an on-line crack monitoring rotor system. Using this methodology, the detection of small levels of damage may be easily undertaken.

Keywords: cracked detection, rotor system, non-linear vibration, super-harmonic components.

1 Introduction

Detection of damage in rotor systems is an important concern to engineering communities. The importance of early detection of cracks has led to continuous efforts due to the fact that unpredictable occurrence of damage may cause catastrophic failure. It is very difficult but also highly desirable to pursue effective engineering solutions to detect and locate the damage situation in rotating systems at the earliest possible stage. Reviews on the dynamical behaviour of rotors with transverse crack were published by Wauer [1], Gasch [2] and Dimarogonas [3].
During the past several decades, significant amount of research has been conducted in the area of crack detection in systems using only theoretical modelling method [4–11], combined both theoretical and experimental methods [12–14] or only experimental method [15]. The main idea of these approaches is that a change in a rotor system due to damage crack will manifest itself as changes in the rotor dynamic behaviour: first of all, the presence of a transverse crack induces a slight decrease of the natural frequencies [2, 10, 16]. Secondly, resonances appear when the rotational speeds of the shaft reach $\frac{1}{2}$ and $\frac{1}{3}$ of the critical speeds of the rotor system. Therefore, with the increase of the crack depth, the $\frac{1}{2}$ and

$\frac{1}{3}$ sub-critical resonant peaks increase [6, 11, 17]. Finally, some researchers [18] indicated that the shaft executes two and three loops per shaft revolution at the $\frac{1}{2}$ and $\frac{1}{3}$ sub-critical speeds, respectively.
In most of the studies for crack detection in rotor systems, researchers used changes in natural frequencies and evolution of the non-linear behaviour of the system at the super-harmonic components as the diagnostic tools. In this paper it will be shown that an appropriate use of the super-harmonic components may be useful for crack detection in rotor systems. So the present study attempts to propose a complete analysis of the crack-unbalance interactions on the super-harmonic components at the $\frac{1}{2}$ and $\frac{1}{3}$ sub-critical resonant peaks. Numerical example will be conducted on variety of damage location, crack size and unbalance parameters (magnitude and relative orientation with the front crack) to verify the suitability of the use of the super-harmonic components in order to detect the presence of a transverse crack in rotor. One of the advantages of the proposed approach is that the emerging of super-harmonic components may be easily undertaken for the detection of a crack in rotating shafts, especially in the early stage of the damage where the ability to discriminate changes of modal parameters caused by damage from those caused by other environmental condition changes is very difficult.
The paper is set up as follows: firstly, the description of the non-linear rotor system and the modeling of the breathing crack are investigated. Then, the non-linear periodic response of the cracked rotor is undertaken by approximating the non-linear dynamic by truncated Fourier series with m harmonics. Moreover, the state vectors of the complete cracked rotor will be partitioned into subvectors relating to the Fourier components which are associated with the degrees of freedom at the crack location, and the Fourier components which are associated with the others degrees of freedom. Then, the emerging of the $2\times$ and $3\times$ super-harmonic components for detecting the presence of a crack is investigated. Numerical examples including various crack parameters (location and depth) and unbalance parameters (magnitude and orientation with the crack) are considered in order to validate the detection of a crack based on the resonance peaks at the $\frac{1}{2}$ or $\frac{1}{3}$ sub-critical resonances and the determination of the associated super-harmonic frequency components.

2 The model of the cracked rotor

In this study, the rotor is composed of a shaft with one disc at the mid-span, as illustrated in Figure 1. All the values of the physical parameters are given in Table 1.

2.1 Shaft elements

The shaft is discretized into 10 Timoshenko beam finite elements with four degrees of freedoms at each node (two lateral displacements and two rotations). At each node of the Timoshenko beam finite elements, we have [19, 20]

$$(\mathbf{M}_T^e + \mathbf{M}_R^e)\,\ddot{\mathbf{X}}^e + (\eta\mathbf{K}_B^e - \omega\mathbf{G}^e)\,\dot{\mathbf{X}}^e + (\mathbf{K}_B^e + \eta\omega\mathbf{K}_C^e)\,\mathbf{X}^e = \mathbf{F}^e \tag{1}$$

where ω is the rotational speed. $\mathbf{M}_T^e$ and $\mathbf{M}_R^e$, and $\mathbf{G}^e$ are the translational, rotary mass and gyroscopic matrices of the shaft element, respectively. $\mathbf{K}_B^e$ and $\mathbf{K}_C^e$ are the stiffness and circulatory matrices due to shaft internal damping. η defines the coefficient of damping that is associated to the modal damping for the first mode of the system at rest ($\omega = 0$). $\mathbf{F}^e$ includes the gravitational forces and unbalance forces.

2.2 Rigid disc

The rotor system has one disc at the mid-span that is modelled as a rigid disk and may be written as

$$\left(\mathbf{M}_T^d + \mathbf{M}_R^d\right)\ddot{\mathbf{X}}^d - \omega\mathbf{G}^d\dot{\mathbf{X}}^d = \mathbf{F}^d \tag{2}$$

where $\mathbf{M}_T^d$ and $\mathbf{M}_R^d$ are the translational mass and rotary mass matrices respectively. $\mathbf{G}^d$ is the gyroscopic matrix, and $\mathbf{F}^d$ corresponds to the unbalance and gravitational forces.

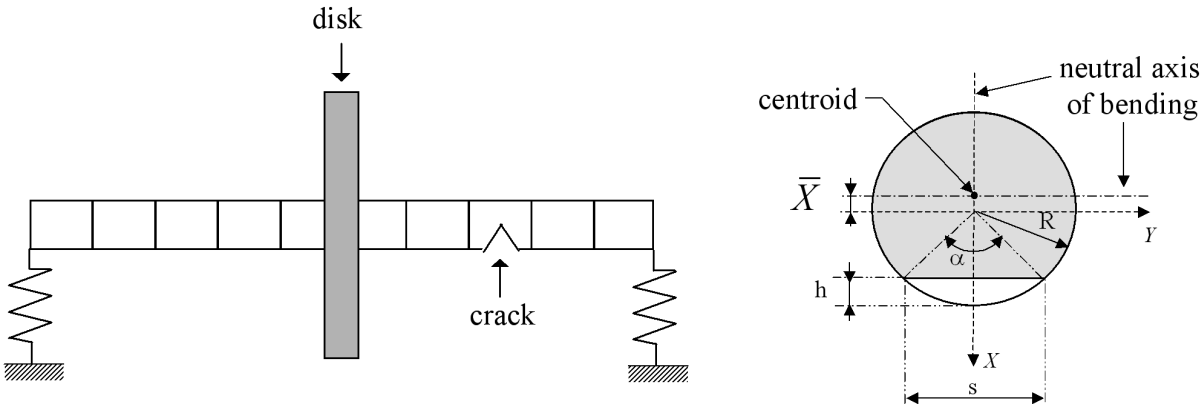

Figure 1: Finite-element model of the rotor and the cracked-beam section

Notation	Description	Value
R	radius of the rotor shaft	$0.005m$
L	length of the rotor shaft	$0.5m$
R_D	outer radius of the disk	$0.025m$
h_D	thickness of the disk	$0.015m$
E	Young's modulus of elasticity	$2.1\ 10^{11}N.m^{-2}$
G	shear modulus	$7.7\ 10^{10}N.m^{-2}$
ρ	density	$7800kg.m^{-3}$
ν	Poisson ratio	0.3
η	coefficient of damping	$2\ 10^{-5}$
m_e	mass unbalance	$0.001kg$
d_e	eccentricity of the mass unbalance	$0.01m$
ϕ	relative orientation between the crack and the unbalance	$0degree$
K_s	stiffness of supports	$2\ 10^6N.m^{-1}$
ω_1, ω_2	first double frequency of the uncracked rotor (at rest)	$317rad.s^{-1}$
ω_3, ω_4	second double frequency of the uncracked rotor (at rest)	$1898rad.s^{-1}$

Table 1: Value of the physical parameters

2.3 Modelling of the breathing crack

2.3.1 The crack model

If a transverse crack appears in a rotor system, additional flexibilities are generated at the location of the crack due to strain energy concentration in the vicinity of the crack tip under load. There are a number of approaches for modelling cracks in shafts; we refer the interested reader to [1] and [3] for comprehensive literature survey of various crack modelling techniques.
In this paper, the model proposed by Mayes and Davies [13, 21] is used in order to locally represent the stiffness properties of the crack cross section. This model considers the reduction of the second moment of area ΔI of the element at the location of the crack that ay be defined by

$$\Delta I = I_0 \left(\frac{\frac{R}{l}\left(1-\nu^2\right) F(\mu)}{1+\frac{R}{l}\left(1-\nu^2\right) F(\mu)} \right) \tag{3}$$

where I_0, R , l, and ν are the second moment of area, the shaft radius, the length of the section and the Poisson's ratio, respectively. μ is the non-dimensional crack depth and is given by $\mu = \frac{h}{R}$ where h defines the crack depth of the shaft. $F(\mu)$ defines the non-linear compliance function varied with the non-dimensional crack depth μ that may be obtained from a series of experiments with chordal cracks [13, 21]. So, the stiffness matrix $\mathbf{K}_{crack}$ of the crack cross section is given by (to the principal axes of the crack front)

$$\mathbf{K}_{crack} = \frac{E}{l^3} \begin{bmatrix} 12I_X & 0 & 0 & 6lI_X & -12I_X & 0 & 0 & 6lI_X \\ & 12I_Y & -6lI_Y & 0 & 0 & -12I_Y & -6lI_Y & 0 \\ & & 4l^2I_Y & 0 & 0 & 6lI_Y & 2l^2I_Y & 0 \\ & & & 4l^2I_X & -6lI_X & 0 & 0 & 2l^2I_X \\ & & & & 12I_X & 0 & 0 & -6lI_X \\ & & & & & 12I_Y & 6lI_Y & 0 \\ & & Sym. & & & & 4l^2I_Y & 0 \\ & & & & & & & 4l^2I_X \end{bmatrix} \tag{4}$$

The moments of inertia about the parallel centroidal axes, I_X and I_Y, are given by [10]

$$I_X = \tilde{I}_X \tag{5}$$

$$I_Y = \tilde{I}_Y - A\bar{X}^2 \tag{6}$$

where $\bar{X}^2$ and A define the uncracked area of the cross-section and the distance from the axis X to the centroid of the cross section

$$\bar{X} = \frac{2}{3A} R^3 \gamma^3 \tag{7}$$

$$A = R^2 \left((1-\mu)\gamma + \frac{\alpha}{2} \right) \tag{8}$$

where α defines the crack angle and is given by $\alpha = 2cos^{-1}(1-\mu)$.
Then, the asymmetric area moments of inertia $\tilde{I}_X$ and $\tilde{I}_Y$ about the X and Y-axes are defined as

$$\tilde{I}_X = \int\int_A Y^2 dA = \frac{R^4}{4} \left((1-\mu)\left(1-4\mu+2\mu^2\right)\gamma + \frac{\alpha}{2} \right) \tag{9}$$

$$\tilde{I}_Y = \int\int_A X^2 dA = \frac{\pi R^4}{4} + R^4 \left(\frac{2}{3}(1-\mu)\gamma^3 + \frac{1}{4}(1-\mu)\left(1 - 4\mu + 2\mu^2\right)\gamma + sin^{-1}(\gamma) \right) \quad (10)$$

where γ is equal to $\sqrt{2\mu - \mu^2}$ for convenience.

2.3.2 The breathing mechanism

When a cracked rotor rotates slowly under the load of its own weight, the crack will open and close once per revolution. This periodic opening and closing of the crack is called " breathing"' phenomenon [8]. Due to this mechanism, the stiffness matrix of the shaft at the crack position is non-linear and periodical time varying during the rotation of the rotor system.
As previously demonstrated by Gasch [2, 16], the opening and closing of the crack during its rotation is mainly due to the shaft self-weight. So, assuming that the static deflection is much greater that the dynamic response of the cracked rotor, the breathing of the crack may be expressed by a cosine function $f(t)$

$$f(t) = \frac{1 - cos\omega t}{2} \quad (11)$$

where ω defines the rotational speed of the rotor.
During the shaft's rotation, the crack opens and closes: the associated breathing action of the crack is illustrated in Figure 2. When the crack is fully closed the rotor may be treated as uncracked, due to the fact that the crack has no effect on the dynamic behaviour of the rotor (i.e. $f(t) = 0$). If $f(t) = 1$, the crack is fully open. As previously explained, this opening and closing of the crack (described in Equation 11) assumes that the gravity determinates the breathing of the crack due to weight dominance (i.e. the static deflection is much greater than the rotor vibration).

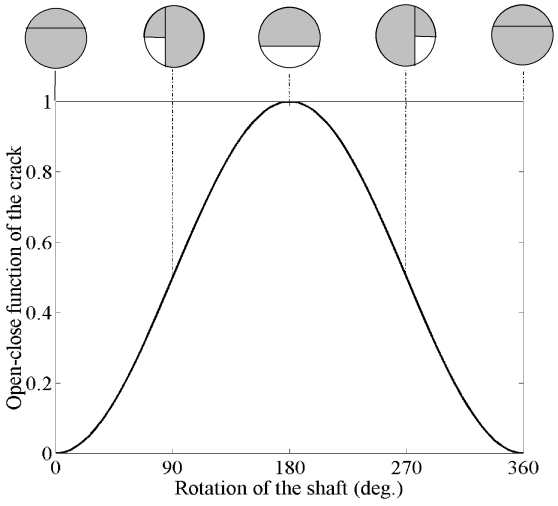

Figure 2: Breathing crack due to the rotation of the shaft (white = portion of opened crack, black=portion of closed crack)

2.4 Equation of motion of the cracked rotor

After assembling the different shaft elements, the rigid disc and the discrete bearing stiffness that are located at the two ends of the shaft, the equation of motion of the complete cracked rotor system in a fixed co-ordinate system can be written as

$$\mathbf{M}\ddot{\mathbf{X}} + \mathbf{D}\dot{\mathbf{X}} + (\mathbf{K} - f(t)\,\mathbf{K}_c)\,\mathbf{X} = \mathbf{Q} + \mathbf{W} \tag{12}$$

where overdots indicate differentiation with respect to time. The mass matrix $\mathbf{M}$ includes mass matrices of the shaft and rigid disc. The matrix $\mathbf{D}$ considers the shaft internal damping, the damping of the supports and the gyroscopic moments. The matrix $\mathbf{K}$ includes the stiffness matrices of the shaft and supports, and the circulatory matrix due to shaft internal damping. $\mathbf{K}_c$ is the stiffness matrix due to the crack. The terms of this matrix are equal to zero except at the crack location degree-of-freedom where the 8×8 matrix $\mathbf{K}_{crack}$ is present. $\mathbf{Q}$ and $\mathbf{W}$ are the vector of gravity and imbalance forces due to the disk and the shaft, respectively.
As previously indicated, the above equations of the cracked rotor have a time-dependent coefficient due to the fact that the crack breathes when the system rotates. The amount of open part of the crack constantly varies with the rotation of the shaft, thereby changing the stiffness of the cracked rotor. The global stiffness matrix of the rotor consists of a constant part $\mathbf{K}$ and a time dependent part $f(t)\,\mathbf{K}_c$.

3 Non-linear analysis

3.1 Non-linear responses of the cracked rotor

Due to the time-dependent coefficient of Equation 12, the system of the crack rotor may be rewritten in a "'non-linear"' form as

$$\mathbf{M}\ddot{\mathbf{X}} + \mathbf{D}\dot{\mathbf{X}} + \mathbf{K}\mathbf{X} = \mathbf{Q} + \mathbf{W} + \mathbf{f}_{NL}(\mathbf{X}, \omega, t) \tag{13}$$

with

$$\mathbf{f}_{NL}(\mathbf{X}, \omega, t) = \frac{1}{2}(1 - cos\omega t)\,\mathbf{K}_c\mathbf{X} \tag{14}$$

In the following the term $\mathbf{f}_{NL}$ will be treated as a non-linear term due to its dependence on $\mathbf{X}$ that makes Equation 13 non-linear. A frequency-domain method such as the harmonic balance methods with continuation schemes that are well-known numerical tools, may be applied in order to study non-linear dynamics vibrations in rotating systems [22, 23]. This approach may be used as an alternative to time-domain methods when periodic solutions of the on-linear system exist, and so is a very efficient way of approximating the vibration of a cracked rotor. We refer the interested reader to [22–25] for a survey of some recent developments and alternative approaches.
The general idea of the harmonic balance method is to represent the periodic solution of the non-linear system by its frequency content.
So, the non-linear dynamical responses of the cracked rotor system are represented as truncated Fourier series with m harmonics:

$$\mathbf{X}(t) = \mathbf{B}_0 + \sum_{k=1}^{m} (\mathbf{B}_k \cos(k\omega t) + \mathbf{A}_k \sin(k\omega t)) \tag{15}$$

where ω defines the fundamental frequency. $\mathbf{B}_0$, $\mathbf{A}_k$ and $\mathbf{B}_k$ (with $k = 1, \cdots, m$) define the unknown coefficients of the finite Fourier series. The number of harmonic coefficients m is selected on the basis

of the number of significant harmonics expected in the non-linear dynamical response.
Moreover, the non-linear force $\mathbf{f}_{NL}$, the gravity force $\mathbf{Q}$ and the global unbalance force $\mathbf{W}$ are represented as truncated Fourier series. First of all, the non-linear force due to the presence of the crack $\mathbf{f}_{NL}$ is approximated by finite Fourier series of order m

$$\mathbf{f}_{NL}\left(\mathbf{X},\omega,t\right)=\mathbf{C}_0^f+\sum_{k=1}^{m}\left(\mathbf{C}_k^f\cos\left(k\omega t\right)+\mathbf{S}_k^f\sin\left(k\omega t\right)\right) \tag{16}$$

Then, it may be observed that the unbalance force components without considering the crack (for the shaft and the disk) in the horizontal and vertical directions (Y-direction and X-direction as indicated in Figure 1) are given as $m_e d_e cos\left(\omega t+\phi\right)$ and $m_e d_e sin\left(\omega t+\phi\right)$, respectively. m_e and d_e are the mass unbalance and the eccentricity for each element of the rotor system. ϕ defines the initial angular position with respect to the Z-axis.
So, the gravity force $\mathbf{Q}$ and the global unbalance force $\mathbf{W}$ are exactly defined by constant components and first-order periodic components in the frequency domain, respectively. We have

$$\mathbf{Q}\left(\mathbf{X},\omega,t\right)=\mathbf{C}_0^Q \tag{17}$$

$$\mathbf{W}\left(\mathbf{X},\omega,t\right)=\mathbf{C}_1^W\cos\left(\omega t\right)+\mathbf{S}_1^W\sin\left(k\omega t\right) \tag{18}$$

Substituting these last fourth expressions 15, 16, 17 and 18 into the rotor equation of motion 13 and balancing the harmonic terms yields a set of $(2m+1)*n$ equations where n is the number of degree-of-freedom for the complete cracked rotor system.
The constant terms $\mathbf{B}_0$ that are given by the first n^{th} relations are given by

$$\mathbf{K}\mathbf{B}_0=\mathbf{C}_0^Q+\mathbf{C}_0^f \tag{19}$$

Then, the first harmonic components $\mathbf{A}_1$ and $\mathbf{B}_1$ are determined by resolving the following equations

$$\left[\begin{array}{cc}\mathbf{K}-\omega^2\mathbf{M} & -\omega\mathbf{D}\\ \omega\mathbf{D} & \mathbf{K}-\omega^2\mathbf{M}\end{array}\right]\left[\begin{array}{c}\mathbf{A}_1\\ \mathbf{B}_1\end{array}\right]=\left[\begin{array}{c}\mathbf{S}_1^W+\mathbf{S}_1^f\\ \mathbf{C}_1^W+\mathbf{C}_1^f\end{array}\right] \tag{20}$$

Finally, the $2m*(n-1)$ remaining equations that define the k^{th} Fourier coefficients $\mathbf{A}_k$ and $\mathbf{B}_k$ for $2\leq k\leq m$ are given by

$$\left[\begin{array}{cc}\mathbf{K}-\left(k\omega\right)^2\mathbf{M} & -k\omega\mathbf{D}\\ k\omega\mathbf{D} & \mathbf{K}-\left(k\omega\right)^2\mathbf{M}\end{array}\right]\left[\begin{array}{c}\mathbf{A}_k\\ \mathbf{B}_k\end{array}\right]=\left[\begin{array}{c}\mathbf{S}_k^f\\ \mathbf{C}_k^f\end{array}\right] \tag{21}$$

The non-linear expression $\mathbf{f}_{NL}\left(\mathbf{X},\omega,t\right)$ is a function of the non-linear responses $\mathbf{X}\left(t\right)$ and the associated Fourier coefficients $\mathbf{B}_0$, $\mathbf{A}_k$ and $\mathbf{B}_k$ (with $1\leq k\leq m$). So, the Fourier coefficients $\mathbf{C}_0^f$, $\mathbf{S}_k^f$ and $\mathbf{C}_k^f$ (with $1\leq k\leq m$) may be determined from $\mathbf{B}_0$, $\mathbf{A}_k$ and $\mathbf{B}_k$ (with $1\leq k\leq m$) by using the following iteration process, called the Alternate Frequency/Time domain approach (AFT method [26])

$$\left[\mathbf{B}_0\ \mathbf{A}_1\ \mathbf{B}_1\ \cdots\ \mathbf{A}_m\ \mathbf{B}_m\right]^T\Rightarrow\quad\mathbf{X}\left(t\right)\ \Rightarrow\ \mathbf{f}_{NL}\left(\mathbf{X},\omega,t\right)\ \Rightarrow\ \left[\mathbf{C}_0\ \mathbf{S}_1\ \mathbf{C}_1\ \cdots\ \mathbf{S}_m\ \mathbf{C}_m\right]^T \tag{22}$$

Then, the $(2m+1)*n$ non-linear equations of motion 19, 20 and 21 can be solved by using a solver such as the Newton-Raphson method [27].
Moreover, a continuation scheme in conjunction with the harmonic balance method and based on the path following continuation and Lagrangian polynomial extrapolation [10, 28], is used to give a first approximation of the Fourier coefficients $\mathbf{B}_0$, $\mathbf{A}_k$ and $\mathbf{B}_k$ (with $1\leq k\leq m$) of the cracked rotor system when the rotational speed ω increases.

3.2 Partition and condensation on the cracked element

The state vectors $\mathbf{A}_k$ and $\mathbf{B}_k$ (for $1 \leq k \leq m$) are partitioned into subvectors relating to the Fourier components $\mathbf{A}_k^c$ and $\mathbf{B}_k^c$ which are associated with the degrees of freedom at the crack location, and the Fourier components $\mathbf{A}_k^u$ and $\mathbf{B}_k^u$ which are associated with the others degrees of freedom.

$$\mathbf{U}_k = \left[\begin{array}{c} \mathbf{U}_k^c \\ \mathbf{U}_k^u \end{array} \right] = \left[\begin{array}{c} \mathbf{A}_k^c \\ \mathbf{B}_k^c \\ \mathbf{A}_k^u \\ \mathbf{B}_k^u \end{array} \right] = \mathbf{\Psi} \left[\begin{array}{c} \mathbf{A}_k \\ \mathbf{B}_k \end{array} \right] \tag{23}$$

The subscript 'k' represents "'k^{th} harmonic components"', the superscript 'u' represents "'uncracked"', and the superscript 'c' represents "'cracked"'.
Hence, for the present case (i.e. the rotor system has only one crack), the vectors $\mathbf{A}_k^c$ and $\mathbf{B}_k^c$ have the size of 8×1, and the vectors $\mathbf{A}_k^u$ and $\mathbf{B}_k^u$ have the size of 36×1. Then, the vectors $\mathbf{U}_k^c$ have the size of 16×1, and the vector $\mathbf{U}_k^u$ have the size of 72×1.
Considering Equation 23, Equation 20 and 21 which is associated with the kth harmonic components can be partitioned as

$$\mathbf{\Theta}_k \mathbf{U}_k = \mathbf{F}_k \tag{24}$$

with

$$\mathbf{\Theta}_k = \left[\begin{array}{cc} \mathbf{\Theta}_k^{cc} & \mathbf{\Theta}_k^{cu} \\ \mathbf{\Theta}_k^{uc} & \mathbf{\Theta}_k^{uu} \end{array} \right] = \mathbf{\Psi}^T \left[\begin{array}{cc} \mathbf{K} - (k\omega)^2 \mathbf{M} & -k\omega \mathbf{D} \\ k\omega \mathbf{D} & \mathbf{K} - (k\omega)^2 \mathbf{M} \end{array} \right] \mathbf{\Psi} \tag{25}$$

Each of the matrices $\mathbf{\Theta}_k$ have the size of 88×88; $\mathbf{\Theta}_k^{cc}$, $\mathbf{\Theta}_k^{cu}$, $\mathbf{\Theta}_k^{uc}$ and $\mathbf{\Theta}_k^{uu}$ are 16×16, 16×72, 72×16, and 72×72 matrices, respectively.
The expressions of $\mathbf{F}_1$ which is associated with the first harmonic components is given by

$$\mathbf{F}_1 = \left[\begin{array}{c} \mathbf{F}_1^c \\ \mathbf{F}_1^u \end{array} \right] = \left[\begin{array}{c} \mathbf{S}_1^{W,c} + \mathbf{S}_1^{f,c} \\ \mathbf{C}_1^{W,c} + \mathbf{C}_1^{f,c} \\ \mathbf{S}_1^{W,u} \\ \mathbf{C}_1^{W,u} \end{array} \right] = \mathbf{\Psi}^T \left[\begin{array}{c} \mathbf{S}_1^W + \mathbf{S}_1^f \\ \mathbf{C}_1^W + \mathbf{C}_1^f \end{array} \right] \tag{26}$$

and the expressions of $\mathbf{F}_k$ (for $2 \leq k \leq m$) which are associated with the k^{th} harmonic components can be rewritten as

$$\mathbf{F}_k = \left[\begin{array}{c} \mathbf{F}_k^c \\ \mathbf{F}_k^u \end{array} \right] = \left[\begin{array}{c} \mathbf{F}_k^c \\ \mathbf{0} \end{array} \right] = \left[\begin{array}{c} \mathbf{S}_k^{f,c} \\ \mathbf{C}_k^{f,c} \\ \mathbf{0} \\ \mathbf{0} \end{array} \right] = \mathbf{\Psi}^T \left[\begin{array}{c} \mathbf{S}_k^f \\ \mathbf{C}_k^f \end{array} \right] \tag{27}$$

The vectors $\mathbf{F}_k$ have the size of 88×1. The vectors $\mathbf{S}_k^{f,c}$, $\mathbf{C}_k^{f,c}$, $\mathbf{S}_1^{W,c}$ and $\mathbf{C}_1^{W,c}$ have the size of 8×1, and the vectors $\mathbf{S}_1^{W,u}$ and $\mathbf{C}_1^{W,u}$ have the size of 36×1.
The vectors $\mathbf{F}_k$ (for $2 \leq k \leq m$) represent the excitation due to the presence of the crack. So the vector $\mathbf{F}_k^u$ is a is a zero vector, as indicated in Equation 27. Moreover, it may be remained that the vector $\mathbf{F}_1$ corresponds not only to the excitation due to the presence of the crack, but also to the contribution of the unbalance force: the terms of this vector are zero except at the crack and unbalance locations. So $\mathbf{F}_1^u$ may only contain an unbalance contribution, as indicated in Equation 26.

So, considering Equations 23, 24, 25 and 26, Equations 20 that define the first harmonic components $\mathbf{A}_1$ and $\mathbf{B}_1$ can be partitioned as

$$\left[\begin{array}{cc} \mathbf{\Theta}_1^{cc} & \mathbf{\Theta}_1^{cu} \\ \mathbf{\Theta}_1^{uc} & \mathbf{\Theta}_1^{uu} \end{array}\right] \left[\begin{array}{c} \mathbf{U}_1^{c} \\ \mathbf{U}_1^{u} \end{array}\right] = \left[\begin{array}{c} \mathbf{F}_1^{c} \\ \mathbf{F}_1^{u} \end{array}\right] \tag{28}$$

Then, considering 23, 24, 25 and 27, the $2m*(n-1)$ Equations 21 that define the k^{th} Fourier coefficients $\mathbf{A}_k$ and $\mathbf{B}_k$ for $2 \leq k \leq m$ may be partitioned as

$$\left[\begin{array}{cc} \mathbf{\Theta}_k^{cc} & \mathbf{\Theta}_k^{cu} \\ \mathbf{\Theta}_k^{uc} & \mathbf{\Theta}_k^{uu} \end{array}\right] \left[\begin{array}{c} \mathbf{U}_k^{c} \\ \mathbf{U}_k^{u} \end{array}\right] = \left[\begin{array}{c} \mathbf{F}_k^{c} \\ \mathbf{0} \end{array}\right] \tag{29}$$

Finally, considering Equations 28 and 29, the vectors $\mathbf{U}_1^c$ and $\mathbf{U}_k^c$ that correspond to the Fourier components of the crack element may be determined by solving

$$\mathbf{U}_1^c = \left(\mathbf{\Theta}_1^{cc} - \mathbf{\Theta}_1^{cu}\mathbf{\Theta}_1^{uu-1}\mathbf{\Theta}_1^{uc}\right)^{-1}\left(\mathbf{F}_1^c - \mathbf{\Theta}_1^{cu}\mathbf{\Theta}_1^{uu-1}\mathbf{F}_1^u\right) \tag{30}$$

$$\mathbf{U}_k^c = \left(\mathbf{\Theta}_k^{cc} - \mathbf{\Theta}_k^{cu}\mathbf{\Theta}_k^{uu-1}\mathbf{\Theta}_k^{uc}\right)^{-1}\mathbf{F}_k^c \tag{31}$$

Then, the Fourier components vectors $\mathbf{U}_1^u$ and $\mathbf{U}_k^u$ of the uncracked elements are given by

$$\mathbf{U}_1^u = \mathbf{\Theta}_k^{uu-1}\mathbf{F}_1^u - \mathbf{\Theta}_k^{uu-1}\left(\left(\mathbf{\Theta}_1^{cc} - \mathbf{\Theta}_1^{cu}\mathbf{\Theta}_1^{uu-1}\mathbf{\Theta}_1^{uc}\right)^{-1}\left(\mathbf{F}_1^c - \mathbf{\Theta}_1^{cu}\mathbf{\Theta}_1^{uu-1}\mathbf{F}_1^u\right)\right) \tag{32}$$

$$\mathbf{U}_k^u = -\mathbf{\Theta}_k^{uu-1}\mathbf{\Theta}_k^{uc}\left(\mathbf{\Theta}_k^{cc} - \mathbf{\Theta}_k^{cu}\mathbf{\Theta}_k^{uu-1}\mathbf{\Theta}_k^{uc}\right)^{-1}\mathbf{F}_k^c \tag{33}$$

4 Numerical simulations

4.1 Effects of the crack size and location

In this section, the main effects of the crack size and location on the non-linear behaviour of the cracked rotor system are briefly summarized.

Firstly, Figures 3 illustrate the effects of crack depth on the vertical and horizontal responses corresponding to the first harmonic component (see Figure 3(a)), the $2\times$ super-harmonic frequency components (see Figure 3(b)), the $2\times$ super-harmonic frequency components (see Figure 3(c)), and the $4\times$ super-harmonic frequency components (see Figure 3(d)) at the node position of the shaft $0.15m$. Due to the presence of the crack, the second harmonic components increase when the rotational speed reaches $\frac{1}{2}$ and 1 of the critical speeds. The third harmonic components (respectively, fourth harmonic components) increase near the rotational speeds at $\frac{1}{3}$, $\frac{1}{2}$ and 1 of the critical speeds (respectively near the rotational speeds at $\frac{1}{4}$, $\frac{1}{3}$, $\frac{1}{2}$ and 1 of the critical speeds). A decrease in the critical speeds of the rotor system due to the reduction in system stiffness resulting from the presence of the crack is also observed. Moreover, it is clear that the vibration amplitudes of the second, third and fourth harmonic components depend on the cracked depth: with the increase of the crack depth, these harmonic components increase. Considering the first harmonic component, the vibration amplitudes of the crack rotor system do not greatly change with respect to the crack size. However, it may be remind that, for a given crack depth, the first harmonic component of the crack rotor system is associated with the rotor imbalance and the relative position between the crack direction and the imbalance [17].

Then, the effects of crack position on the harmonic components of the nonlinear response of the rotor are

illustrated in Figures 4. It may be remind that the crack location clearly affect the decrease in the critical speeds of the cracked rotor and the vibration amplitudes in the sub-critical resonances [11]. Finally, it may be observed that antiresonances for the $2\times$, $3\times$ and $4\times$ super-harmonic frequency components of the cracked rotor system appears due to the presence of the crack. The emerging and location of new antiresonances and the shift in the antiresonances depend on the crack size and location.
In conclusion, the variation of non-linear responses and the emerging of new resonance - antiresonance peaks of the cracked rotor at second, third and fourth harmonic components may provide useful information on the presence of a crack and may be used on an on-line crack monitoring rotor system.

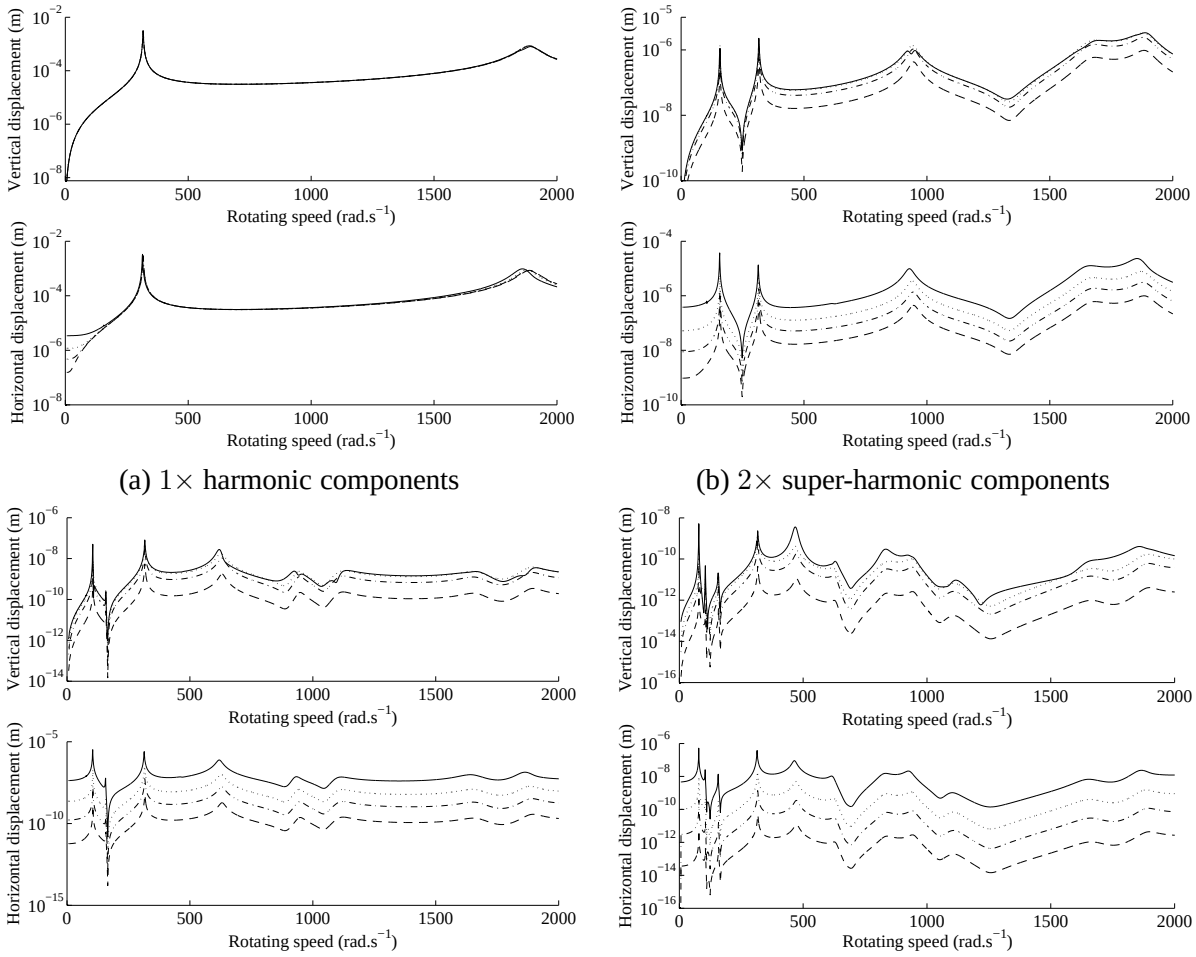

(a) $1\times$ harmonic components

(b) $2\times$ super-harmonic components

(c) $3\times$ super-harmonic components

(d) $4\times$ super-harmonic components

Figure 3: Effects of the crack size at the node position of the shaft $0.15m$ with a crack situated at $L_{crack} = 0.175m$ and the unbalance located at $0.1m$ of the left end ($-$ $\mu = 1$, ... $\mu = 0.75$, $-.-$ $\mu = 0.5$, $- -$ $\mu = 0.25$)

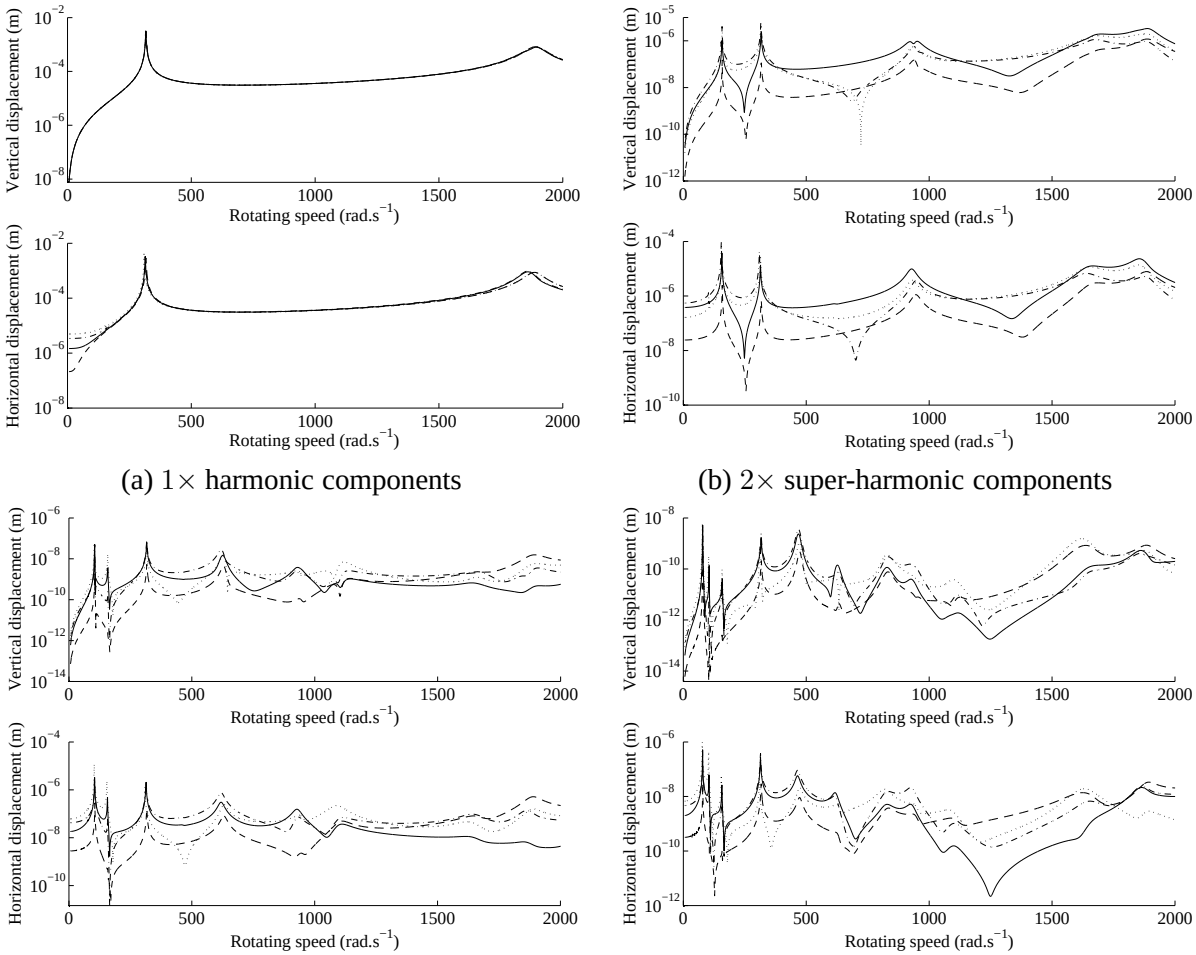

(a) $1\times$ harmonic components

(b) $2\times$ super-harmonic components

(c) $3\times$ super-harmonic components

(d) $4\times$ super-harmonic components

Figure 4: Effects of the crack location at the node position of the shaft $0.15m$ with a non-dimensional crack depth $\mu = 1$ and the unbalance located at $0.1m$ of the left end (position of the crack $--L_{crack} = 0.075m$, $-L_{crack} = 0.125m$, $-.-L_{crack} = 0.175m$, $...L_{crack} = 0.225m$)

4.2 Damping and unbalance effects

First of all, it is well known that increasing the rotor unbalance increases the $1\times$ amplitudes of the cracked rotor [17]: this fact is indicated in Equations 28 and 20. However, it may be noted that the other $n\times$ amplitudes (with $n \geq 2$) may also be affected by the rotor imbalance. Figure 5(a) illustrates the evolution of the vibration amplitudes in the $\frac{1}{2}$ sub-critical resonances with the variation of the unbalance of the cracked rotor. With the increase of the rotor unbalance, the amplitudes at the sub-critical resonances increase, due to the interaction of the crack breathing mechanism, gravity and rotor unbalance (as indicated in Equations 29 and 21). Effectively, it may be remained that the amplitudes of the non-linear terms 16 due to the presence of the crack depend on the amplitudes of the rotor's vertical and horizontal displacements (as indicated in Equation 14) and so the rotor unbalance.
Moreover, the vibration amplitudes in the $\frac{1}{2}$ sub-critical resonances depend on the damping of the cracked rotor system, as illustrated in Figure 5(b). With any decrease of damping, the amplitudes increase drastically and the presence of the crack may be clearly detected. However, if the damping of the rotor system is relatively high, the resonant amplitudes in the $\frac{1}{2}$ sub-critical resonances will disappear due to the fact that the $2\times$ and $3\times$ super-harmonic frequency components are suppressed. These informations can be used as indexes for the detection of cracks in the rotor system: if the damping remains constant, increasing the unbalance of the rotor system may change and increase the $n\times$ amplitudes (with $n \geq 2$) when the rotor reaches the $\frac{1}{n}$ sub-critical resonances.

However, it is clear that the vibration amplitudes in the $\frac{1}{n}$ sub-critical resonances (with $n \geq 2$) depend not only on the rotor damping, unbalance, position and depth of the crack, but also on the combinations of the unbalance and the crack parameters. So, the effects of crack-unbalance interaction are analysed in the following section of this paper.

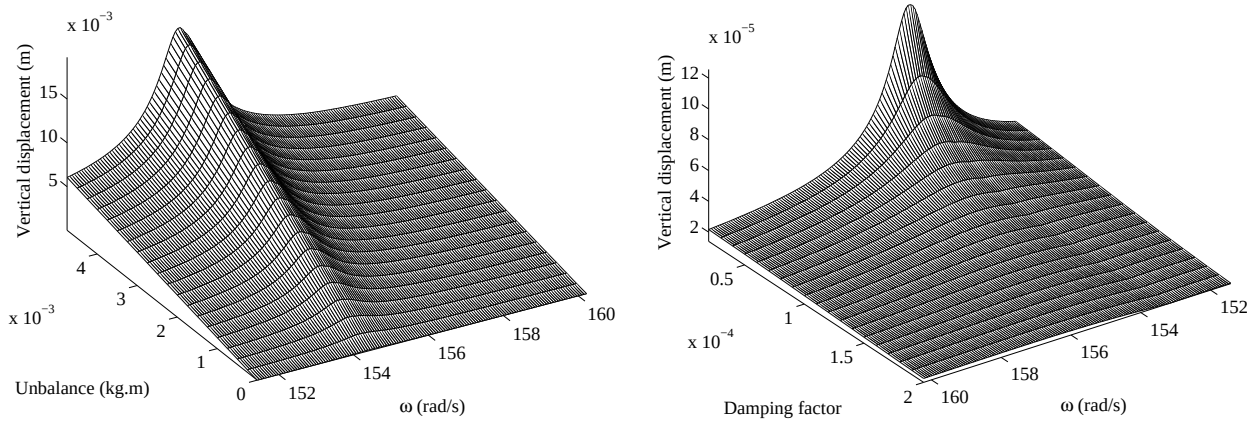

(a) Unbalance effect (b) Damping effect

Figure 5: Influence of damping and mass unbalance on the vertical vibration amplitudes around $\frac{1}{2}$ sub-critical resonances (with $\mu = 1$, $L_{crack} = 0.225m$) and the unbalance located at $0.25m$

4.3 Effects of the crack-unbalance interaction on the super-harmonic frequency components

Figures 7 illustrate the second super-harmonic frequency components of the middle of the rotor for various crack-unbalance orientations and unbalance in the vertical and horizontal directions. It clearly appears that the relative orientation angle between the unbalance of the cracked rotor and the crack and their interaction drastically affect the evolutions of the second super-harmonic frequency component at the $\frac{1}{2}$ sub-critical resonances. Then, the evolutions of the $\frac{1}{2}$ sub-critical resonances peak with respect to the unbalance-crack angle change due to the magnitude of the unbalance in both the vertical and horizontal directions (see for example Figures 7(b), (d) and (f)).
Therefore, it may be observed that the interaction between the crack and the unbalance may mask the presence of the crack: effectively, the second super-harmonic frequency component and the resonant amplitudes in the $\frac{1}{2}$ sub-critical resonances may disappear (see for example Figure 7(b) when the angle of the unbalance is at 270 degrees).
Figures 6 indicate the evolutions of the third super-harmonic components of the middle of the rotor when the rotor reaches the $\frac{1}{3}$ sub-critical resonances. As previously seen for the second super-harmonic frequency component, depending on the relative angle between unbalance and crack vectors, the third super-harmonic frequency component can increase or even decrease in vertical and horizontal amplitudes. With the decrease of the rotor unbalance, the magnitudes of the super-harmonic frequency components decrease in the vertical and horizontal directions. If the crack effect is predominant, the magnitude of the sub-critical resonances peaks does not greatly change, as illustrated in Figures 7(e-f) and 6(e-f). If the crack unbalance is more important than the crack, it is well known that the the magnitude of the sub-critical resonances peaks is constant as shown in Figure 7(a) for the horizontal direction. However, it may be noted that the associated magnitude of the sub-critical resonances peak slightly changes in the vertical direction: effectively, the highest changes in the stiffness of the crack cross section (see Equation 4) occur in the vertical direction due to the orientation of the crack and the shaft self-height. This is why the sensibility of the magnitudes of $\frac{1}{2}$ and $\frac{1}{3}$ sub-critical resonances with respect to the unbalance angle and the unbalance-crack interactions are different in the vertical and horizontal directions.
Moreover, the influence of the crack on the non-linear dynamic of the rotor system increases when the unbalance magnitude decreases. In this case, two resonant peaks appear in the horizontal direction due the coupling between the two bending directions, as indicated in Figure 7(e). With the decrease of the unbalance, the ratio between the first resonance peak (at $103rad/s$) and the second resonance peak (at $105rad/s$) decreases (see Figures 7(a), (c) and (e)). The same phenomenon is observed at the $\frac{1}{3}$ sub-critical resonances, as indicated in Figures 6(a), (c) and (e). It may be noted that the crack-imbalance magnitudes and relative angle are not known a priori, making crack detection very difficult. All these information can be used to identify the crack-unbalance interaction and the predominance of the crack or unbalance on the dynamic of the rotor system.
In conclusion, for a given crack depth and position, the magnitudes of the second and third super-harmonic frequency components (at the $\frac{1}{2}$ and $\frac{1}{3}$ sub-critical resonances, respectively) are associated with the rotor unbalance and the position of the unbalance relative to the front crack direction. With the decrease and increase of the rotor unbalance, the magnitudes of the second and third super-harmonic components in both the vertical and horizontal directions may drastically change due to the interaction of gravity, the rotor unbalance and the crack breathing action.
All these phenomena may also be observed for first order harmonic frequency components of the first critical speed, as illustrated in Figure 8(a), but also for the super-harmonic frequency components of the second critical speed of the cracked rotor, as indicated in Figure 8(b): the rotor unbalance and the

position of the unbalance relative to the crack direction greatly influence the maximum of the resonance peak at the critical speed and the second super-harmonic frequency components of the second critical speed.

4.4 Effects of the crack-unbalance orientation and crack depth

In this section the influence of the crack depth with the interaction of the crack-unbalance orientation is investigated. For the sake of clarity, we focus the study at the $\frac{1}{3}$ sub-critical resonances. Figures 9 show the third super-harmonic frequency components of the degree-of-freedom situated at the middle of the rotor, for various crack-unbalance orientations and three non-dimensional crack depth. These figures may be compared with the Figures 6(c) and (d) of the previous section (with a non-dimensional crack depth that is equal to $\mu = 1$, corresponding to the loss of half the shaft's area).
Due to the crack depth and the crack-unbalance interaction, the magnitudes of the third super-harmonic frequency components at $\frac{1}{3}$ sub-critical resonances of the first critical speed change: with the decrease of the non-dimensional crack depth, the influence of the crack is less predominant in the horizontal direction. Moreover, the value of the associated resonance peak decreases with the increase of the crack due to the reduction of the second moment of area at the location of the crack. For a deep crack ($\mu = 1$ in Figure 6(c)), two resonance peaks appear due to the breathing crack and the associated coupling between the horizontal and vertical direction. When the crack depth decreases, the first resonance peak disappear (as shown for $\mu = 0.75$ in Figure 9(a)).
Then, the crack-unbalance interaction is more predominant in the vertical direction: when the crack depth decrease, the ratio between the minimum and maximum of the third super-harmonic frequency components (as a function of the orientation between the crack and the unbalance) decrease or increase. This reflects the fact that for a deep crack, the crack effect is predominant, whereas the unbalance effect is more important when the crack depth is small.
All these results illustrate that the detection of a crack can be difficult due to the interaction of the effects of the crack and the unbalance. However, the influence of the orientation between the crack and the unbalance appear to be clearly identified if the evolutions of the $n\times$ super-harmonic frequency components at the $\frac{1}{n}$ sub-critical resonances are investigated. It may be observed that the classical non-linear responses of the cracked rotor at the $\frac{1}{2}$ or $\frac{1}{3}$ sub-critical resonances may be very complex, as indicated in Figures 10. Effectively, the evolution of the complete non-linear magnitudes as a function of the relative orientation angle between unbalance and the crack and their interaction drastically affect the system response, making crack detection very difficult. The magnitudes of the $\frac{1}{2}$ or $\frac{1}{3}$ sub-critical resonances correspond to the combination of all the harmonic components. So these evolutions of resonance peaks do not permit a vibration characterization of the cracked rotor system due to the influence and interaction between all the super-harmonic frequency components.

5 Conclusion

The evolution of the super-harmonic components of $2\times$ and $3\times$ revolution in the sub-critical speed region can be used as an index to detect a crack in the rotor. However, due to crack-unbalance interaction the evolutions of the super-harmonic frequency components and the associated resonance peaks may be very complex. It was demonstrated that for a given crack depth, the unbalance does not only affect the vibration amplitude of the $1\times$ amplitudes, but also the $\frac{1}{2}$ and $\frac{1}{3}$ sub-critical resonant peaks. With the increase of the unbalance magnitude, the $\frac{1}{n}$ sub-critical resonant peaks increase obviously due to the non-linear behaviour of the breathing crack and the interaction between the crack, gravity and unbalance

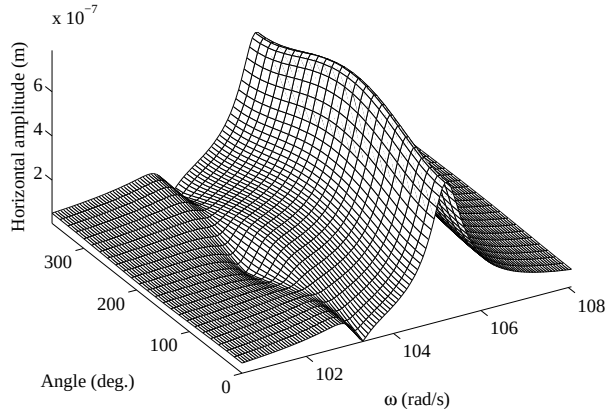

(a) Horizontal amplitudes - $m_e d_e = 10^{-4} kg.m$

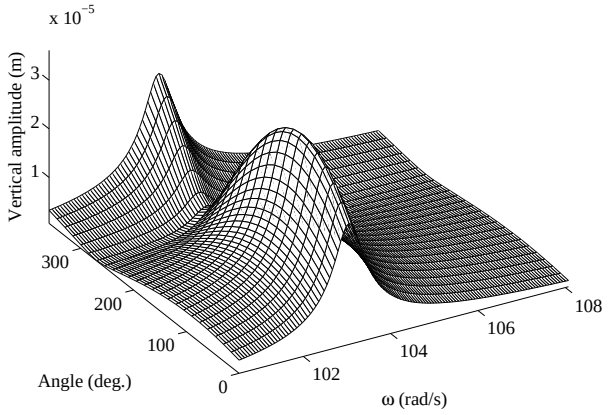

(b) Vertical amplitudes - $m_e d_e = 10^{-4} kg.m$

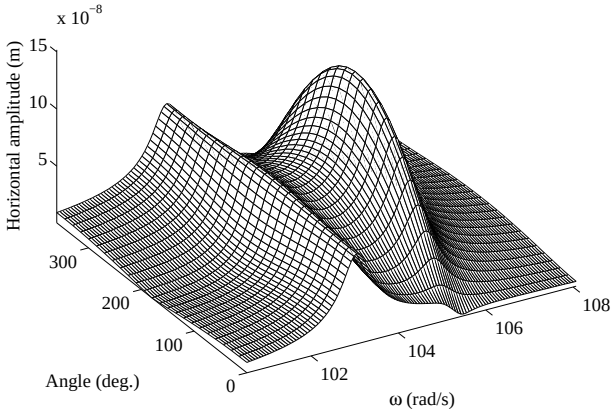

(c) Horizontal amplitudes - $m_e d_e = 10^{-5} kg.m$

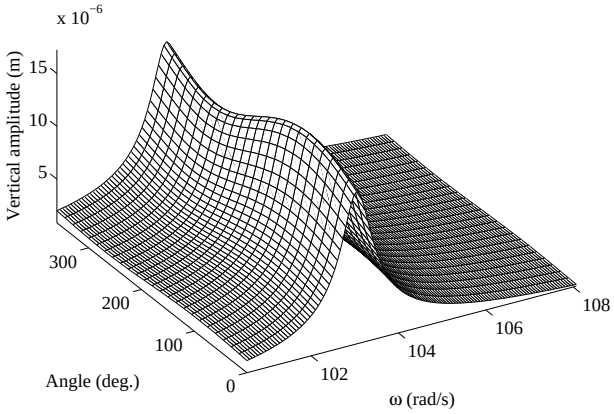

(d) Vertical amplitudes - $m_e d_e = 10^{-5} kg.m$

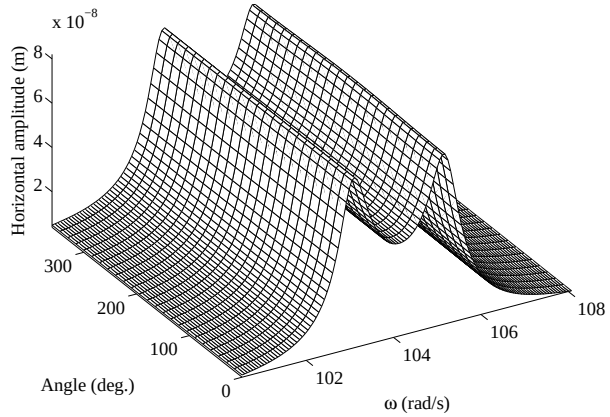

(e) Horizontal amplitudes - $m_e d_e = 10^{-7} kg.m$

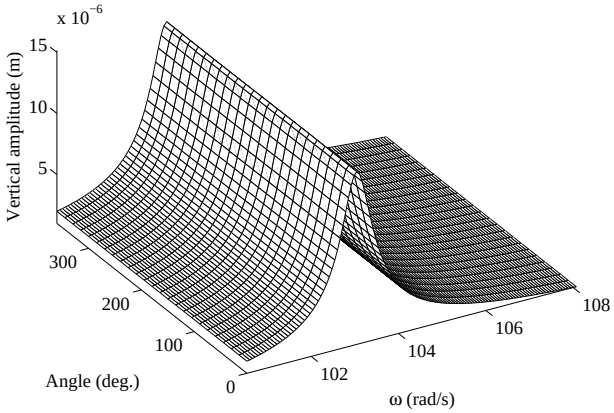

(f) Vertical amplitudes - $m_e d_e = 10^{-7} kg.m$

Figure 6: Evolution of the $3\times$ super-harmonic frequency components on the $\frac{1}{3}$ sub-critical resonances (at the middle of the shaft $0.25m$) with respect to the crack-unbalance orientation (with $\mu = 1$, $L_{crack} = 0.225m$ and the unbalance located at $0.25m$)

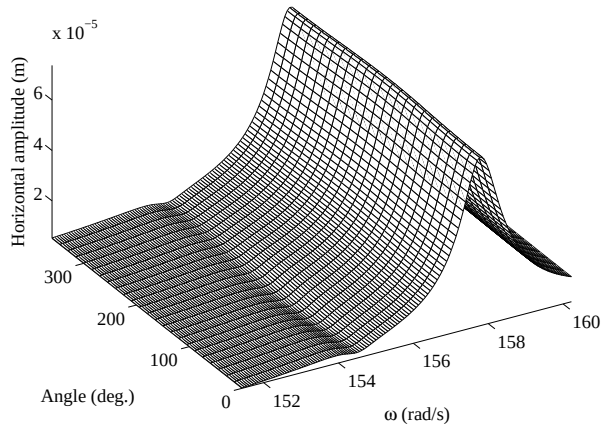

(a) Horizontal amplitudes - $m_e d_e = 10^{-4} kg.m$

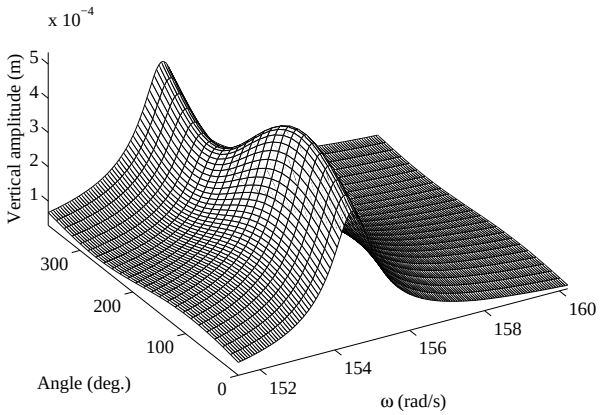

(b) Vertical amplitudes - $m_e d_e = 10^{-4} kg.m$

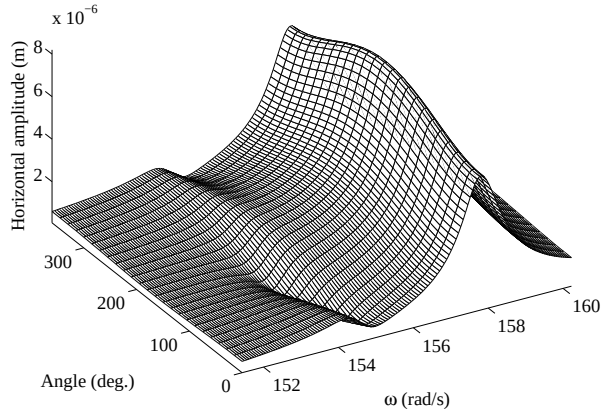

(c) Horizontal amplitudes - $m_e d_e = 10^{-5} kg.m$

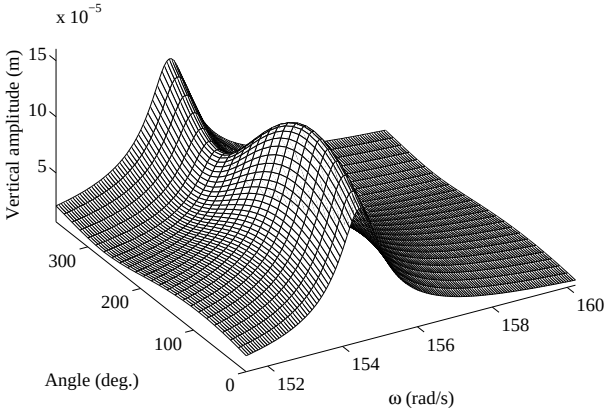

(d) Vertical amplitudes - $m_e d_e = 10^{-5} kg.m$

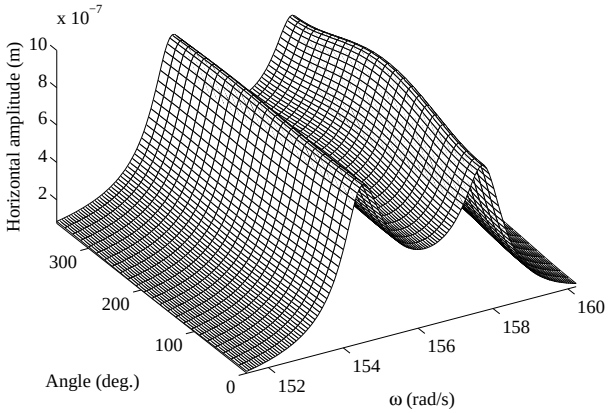

(e) Horizontal amplitudes - $m_e d_e = 10^{-7} kg.m$

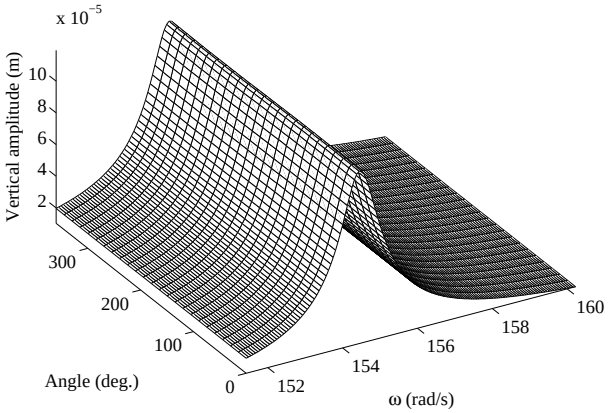

(f) Vertical amplitudes - $m_e d_e = 10^{-7} kg.m$

Figure 7: Evolution of the $2\times$ super-harmonic frequency components on the $\frac{1}{2}$ sub-critical resonances (at the middle of the shaft $0.25m$) with respect to the crack-unbalance orientation (with $\mu = 1$, $L_{crack} = 0.225m$ and the unbalance located at $0.25m$)

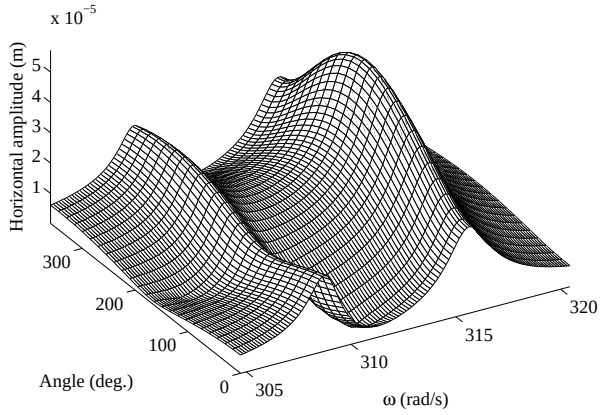

(a) $\mu = 1$, $L_{crack} = 0.225m$, $m_e d_e = 10^{-7} kg.m$

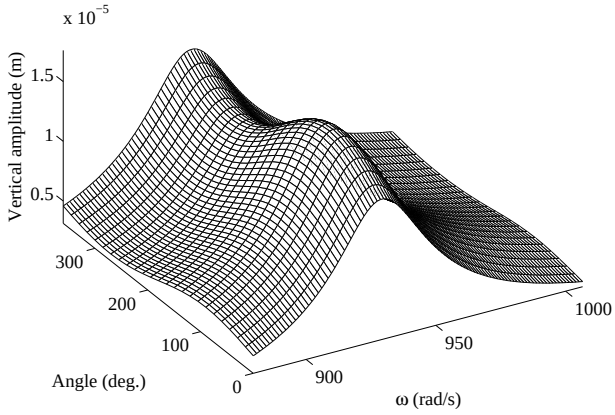

(b) $\mu = 1$, $L_{crack} = 0.125m$, $m_e d_e = 10^{-5} kg.m$

Figure 8: Evolution of the amplitudes with respect to the crack-unbalance orientation (a) at the middle of the shaft $0.25m$ for the first harmonic frequency components in the first critical speed with the unbalance located at $0.25m$, (b) at the one third of the shaft $0.15m$ for the $2\times$ super-harmonic frequency components in the $\frac{1}{2}$ sub-critical resonances of the second critical speed with the unbalance located at $0.15m$

of the rotor.
Even if the crack-unbalance orientation and the unbalance magnitude are unknown, both $2\times$ and $3\times$ super-harmonic frequency components can be used to detect the presence of crack in rotor. The suitability of this approach was verified for various numerical example on a variety of damage location, crack size, unbalance magnitude, and crack size orientation. It appears that the detection of the resonances peaks at the $\frac{1}{2}$ or $\frac{1}{3}$ sub-critical resonances and the determination of the associated super-harmonic frequency components may be useful and acceptable to the industrial community.

References

[1] Wauer, J., 1990. "Dynamics of cracked rotors: Literature survey". *Applied Mechanics Review,* **43**, pp. 13–17 .

[2] Gasch, R., 1993. "A survey of the dynamic behaviour of a simple rotating shaft with a transverse crack". *Journal of Sound and Vibration,* **160(2)**, pp. 313–332.

[3] Dimarogonas, A., 1996. "Vibration of cracked structures: a state of the art review". *Engineering Fracture Mechanics,* **55**, p. 831–857.

[4] Sekhar, A., 2004. "Crack identification in a rotor system:a model-based approach". *Journal of Sound and Vibration,* **270**, p. 887–902.

[5] Gounaris, G. D., and Papadopoulos, C. A., 2002. "Crack identification in rotating shafts by coupled response measurements". *Engineering Fracture Mechanics,* **69**, p. 339–352.

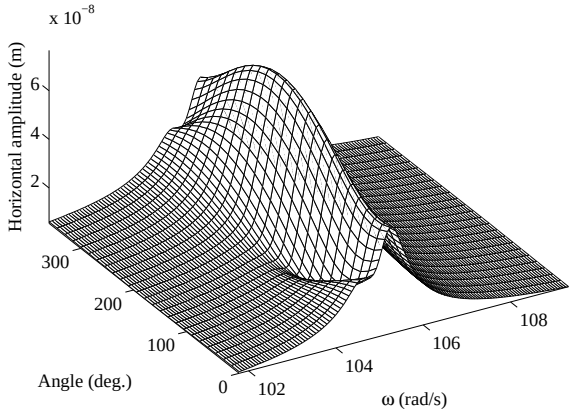

(a) Horizontal amplitudes - $\mu = 0.75$

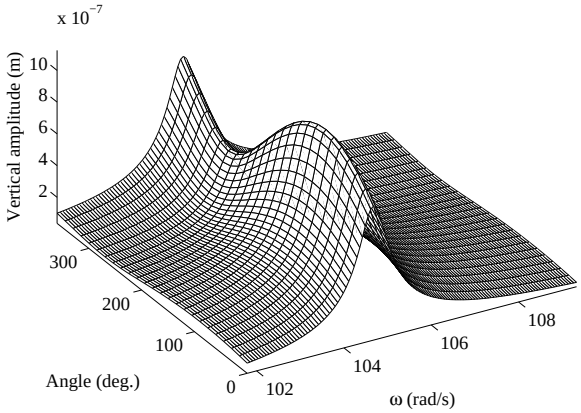

(b) Vertical amplitudes - $\mu = 0.75$

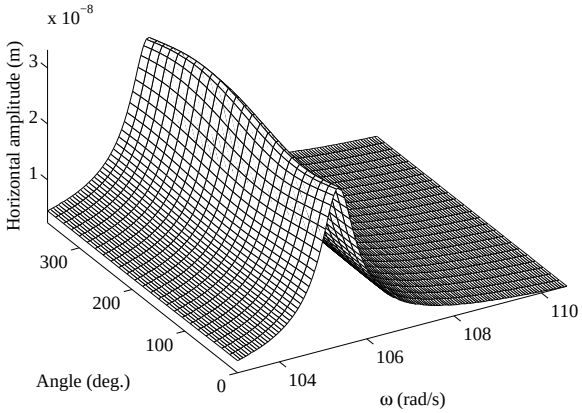

(c) Horizontal amplitudes - $\mu = 0.5$

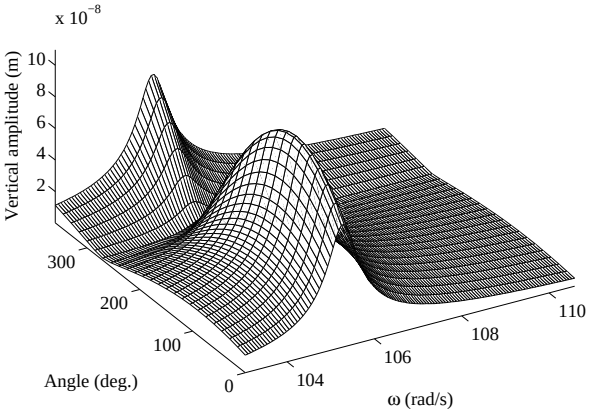

(d) Vertical amplitudes - $\mu = 0.5$

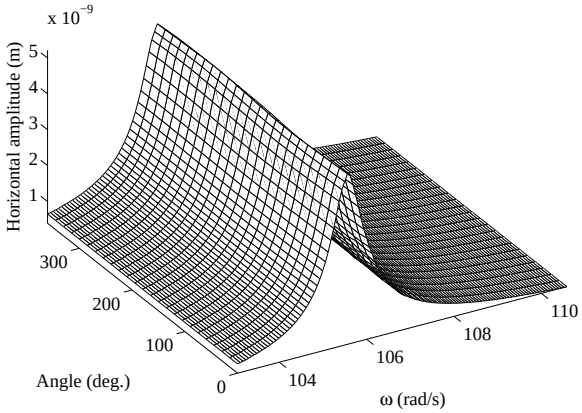

(e) Horizontal amplitudes - $\mu = 0.25$

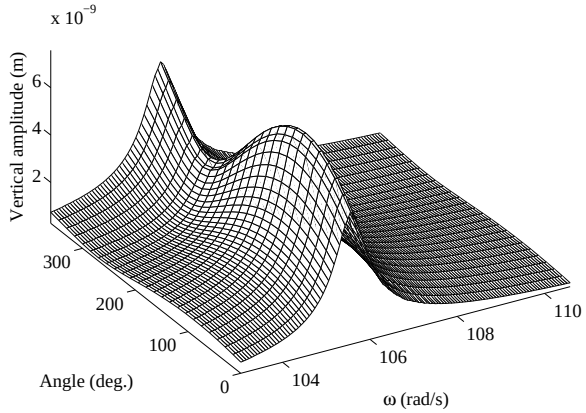

(f) Vertical amplitudes - $\mu = 0.25$

Figure 9: Evolution of the $3\times$ super-harmonic frequency components in the $\frac{1}{3}$ sub-critical resonances (at the middle of the shaft $0.25m$) with respect to the crack-unbalance orientation and the non-dimensional crack depth (with $L_{crack} = 0.225m$, $m_e d_e = 10^{-5} kg.m$ and the unbalance located at $0.25m$)

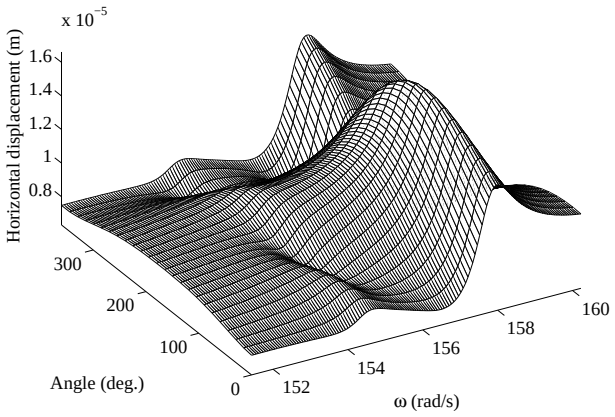

(a) Horizontal amplitudes - $m_e d_e = 10^{-5} kg.m$

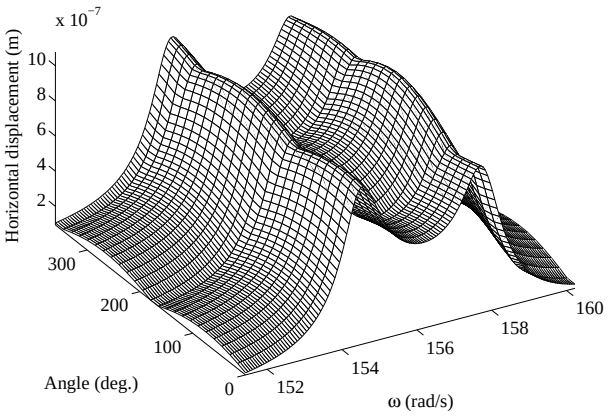

(b) Horizontal amplitudes - $m_e d_e = 10^{-7} kg.m$

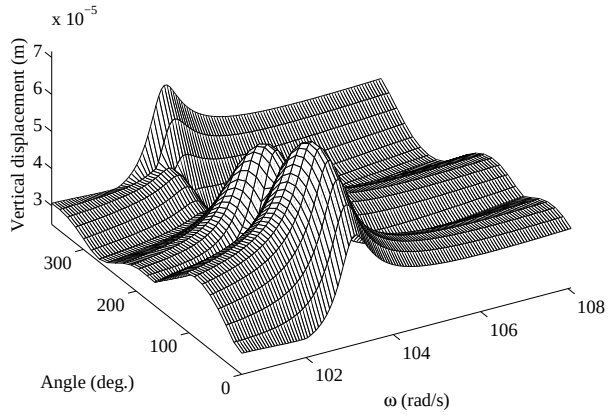

(c) Vertical amplitudes - $m_e d_e = 10^{-4} kg.m$

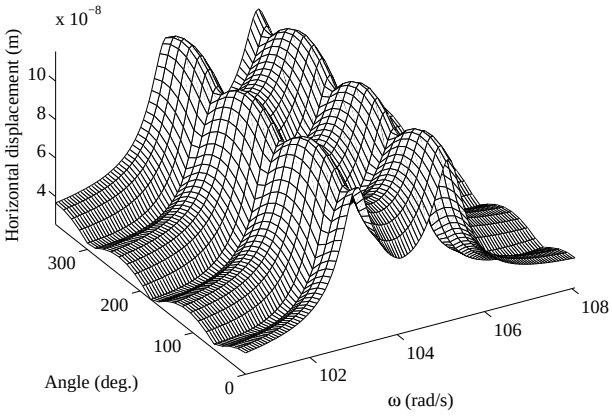

(d) Horizontal amplitudes - $m_e d_e = 10^{-7} kg.m$

Figure 10: Evolutions of the non-linear responses (a-b) $\frac{1}{2}$ sub-critical resonances $\frac{1}{2}$, (c-d) $\frac{1}{3}$ sub-critical resonances (with $L_{crack} = 0.225m$ and $\mu = 1$)

[6] Chen, C., Dai, L., and Fu, Y., 2006. "Nonlinear response and dynamic stability of a cracked rotor". *Communications in Nonlinear Science and Numerical Simulation,* **In press**, p. 15.

[7] Prabhakar, S., Sekhar, A., and Mohanty, A., 2002. "Transient lateral analysis of a slant-cracked rotor passing through its flexural critical speed". *Mechanism and Machine Theory 37 (2002) 1007–1020,* **37**, p. 1007–1020 .

[8] Friswell, M., and Penny, J., 2002. "Crack modelling for structural health monitoring". *International Journal of Structural Health Monitoring,* **1 (2)**, p. 139–148.

[9] Pugno, N., Surace, C., and Ruotolo, R., 2000. "Evaluation of the non-linear dynamic response to harmonic excitation of a beam with several breathing cracks". *Journal of Sound and Vibration,* **235 (5)**, p. 749–762.

[10] Sinou, J.-J., and Lees, A. W., 2005. "Influence of cracks in rotating shafts". *Journal of Sound and Vibration,* **285(4-5)**, pp. 1015–1037.

[11] Sinou, J.-J., and Lees, A. W., 2007. "A non-linear study of a cracked rotor". *European Journal of Mechanics A/Solids,* **26(1)**, pp. 152–170.

[12] Mayes, I., and Davies, W., 1976. "The vibrational behaviour of a rotatingsystem containinga transverse crack". *IMechE Conference on Vibrations in Rotating Machinery,* **C/168/76**, pp. 53–64.

[13] Mayes, I. W., and Davies, W. G. R., 1984. "Analysis of the response of a multi-rotor-bearing system containing a transverse crack in a rotor". *Transactions of the ASME Journal of Vibration, Acoustics, Stress, and Reliability in Design,* **106**, pp. 139–145.

[14] P. Pennacchi, N. Bachschmid, A. V., 2006. "A model-based identification method of transverse cracks in rotating shafts suitable for industrial machines". *Mechanical Systems and Signal Processing,* **In press**, p. 36.

[15] Adewusi, S., and Al-Bedoor, B., 2002. "Experimental study on the vibration of an overhung rotor with a propagating transverse crack". *Shock and Vibration,* **9**, p. 91–104.

[16] Gasch, R., 1976. "Dynamic behaviour of a simple rotor with a cross-sectional crack". *IMechE Conference on Vibrations in Rotating Machinery,* **C/178/76**, p. 123–128.

[17] Zhu, C., Robb, D., and Ewins, D., 2003. "The dynamics of a cracked rotor with an active magnetic bearing". *Journal of Sound and Vibration,* **265**, p. 469–487.

[18] Henry, T., and Okah, B., 1976. "Vibration in cracked shafts". *IMechE Conference on Vibrations in Rotating Machinery,* **C/162/76**, p. 15–19.

[19] Nelson, H., and Nataraj, C., 1986. "The dynamics of a rotor system with a cracked shaft". *Journal of Vibration, Acoustics, Stress, and Reliability in Design,* **108**, p. 189–196.

[20] Lalanne, M., and Ferraris, G., 1990. *Rotordynamics Prediction in Engineering,* 2 ed. John Wilet and Sons.

[21] Davies, W. G. R., and Mayes, I. W., 1984. "The vibrational behaviour of a multi-shaft, multi-bearing system in the presence of a propagating transverse crack". *Transactions of the ASME Journal of Vibration, Acoustics, Stress, and Reliability in Design,* **106**, pp. 146–153.

[22] Nayfeh, A., and Balachandran, B., 1995. *Applied nonlinear dynamics : analytical, computational and experimental methods*. John Wiley & Sons.

[23] Nayfeh, A., and Mook, D., 1995. *Nonlinear oscillations*. John Wiley & Sons.

[24] He, J., 2006. "Some asymptotic methods for strongly nonlinear equations". *International Journal of Modern Physics B*, **20(10)**, pp. 1141–1199.

[25] Sinou, J.-J., Thouverez, F., and Jézéquel, L., 2004. "Methods to reduce non-linear mechanical systems for instability computation". *Archives of Computational Methods in Engineering: State of the Art Reviews*, **11(3)**, pp. 257–344.

[26] Cameron, T. M., and Griffin, J. H., 1989. "An alternating frequency time domain method for calculating the steady state response of nonlinear dynamic systems". *ASME Journal of Applied Mechanics*, **56**, pp. 149–154.

[27] Flannery, B. P., Teukolsky, S. A., and Vetterling, W., 1992. *Numerical Recipes in Fortran*, 2 ed. Cambridge University Press.

[28] Cardona, A., Lerusse, A., and Geradin, M., 1998. "Fast fourier nonlinear vibration analysis". *Computational Mechanics*, **22**, pp. 128–142 .